JBC RESEARCH ARTICLE

Polyunsaturated fatty acids promote the rapid fusion of lipid droplets in *Caenorhabditis elegans*

Received for publication, January 23, 2022, and in revised form, June 7, 2022 Published, Papers in Press, June 23, 2022,
https://doi.org/10.1016/j.jbc.2022.102179

Yanli Wang[1,‡], Chunxia Li[1,‡], Jingjing Zhang[1,‡], Xiumei Xu[1], Lin Fu[1], Jie Xu[2], Hong Zhu[1], Ying Hu[3], Chengbin Li[1], Mengjie Wang[1], Yingjie Wu[4,5,*], Xiaoju Zou[3,*], and Bin Liang[1,*]

From the [1]Center for Life Sciences, School of Life Sciences, State Key Laboratory for Conservation and Utilization of Bio-Resources, Yunnan University, Kunming, Yunnan, China; [2]Key Laboratory of Animal Models and Human Disease Mechanisms of the Chinese Academy of Sciences & Yunnan province, Kunming Institute of Zoology, CAS, Kunming, Yunnan, China; [3]College of Chinese Materia Medica and Yunnan Key Laboratory of Southern Medicinal Utilization, Yunnan University of Chinese Medicine, Kunming, Yunnan, China; [4]Shandong Provincial Hospital, School of Laboratory Animal & Shandong Laboratory Animal Center, Science and Technology Innovation Center, Shandong First Medical University & Shandong Academy of Medical Sciences, Jinan, Shandong, China; [5]Institute for Genome Engineered Animal Models of Human Diseases, National Center of Genetically Engineered Animal Models for International Research, Liaoning Provence Key Lab of Genome Engineered Animal Models Dalian Medical University, Dalian, Liaoning, China

Edited by Qi-Qun Tang

Lipid droplets (LDs) are intracellular organelles that dynamically regulate lipids and energy homeostasis in the cell. LDs can grow through either local lipid synthesis or LD fusion. However, how lipids involving in LD fusion for LD growth is largely unknown. Here, we show that genetic mutation of *acox-3* (acyl-CoA oxidase), *maoc-1* (enoyl-CoA hydratase), *dhs-28* (3-hydroxylacyl-CoA dehydrogenase), and *daf-22* (3-ketoacyl-CoA thiolase), all involved in the peroxisomal β-oxidation pathway in *Caenorhabditis elegans*, led to rapid fusion of adjacent LDs to form giant LDs (gLDs). Mechanistically, we show that dysfunction of peroxisomal β-oxidation results in the accumulation of long-chain fatty acid-CoA and phosphocholine, which may activate the sterol-binding protein 1/sterol regulatory element–binding protein to promote gLD formation. Furthermore, we found that inactivation of either FAT-2 (delta-12 desaturase) or FAT-3 and FAT-1 (delta-15 desaturase and delta-6 desaturase, respectively) to block the biosynthesis of polyunsaturated fatty acids (PUFAs) with three or more double bonds (n≥3-PUFAs) fully repressed the formation of gLDs; in contrast, dietary supplementation of n≥3-PUFAs or phosphocholine bearing these PUFAs led to recovery of the formation of gLDs in peroxisomal β-oxidation–defective worms lacking PUFA biosynthesis. Thus, we conclude that n≥3-PUFAs, distinct from other well-known lipids and proteins, promote rapid LD fusion leading to LD growth.

Lipid droplets (LDs) are intracellular organelles present in some prokaryotes and almost all eukaryotic cells from yeast to humans. Distinguished from other organelles, LDs have a unique architecture consisting of a neutral lipids core, mainly enriched in triacylglycerols (TAGs) and sterol esters, which is wrapped by a phospholipid (PL) monolayer decorated with LD proteins (1–3). In cells, the main function of LDs is to dynamically regulate energy homeostasis through a fascinating cycle of biogenesis and consumption in response to energy surplus or requirement (4). Disturbance of this homeostasis often leads to many human metabolic disorders, including insulin resistance, type 2 diabetes, fatty liver disease, cardiovascular diseases, and so on, which are prevalent diseases threatening human health worldwide.

The lipid storage capacity of LDs is controlled by its growth *via* local lipid synthesis or by LD fusion (5). It is widely accepted that the LDs are initiated and nascent LDs are formed from the endoplasmic reticulum (ER) (6–8). The nascent LDs may grow to mature ones by acquiring neutral lipids from the ER through a continuous association with the ER (9–12). Alternatively, after the nascent LDs bud from the ER, LD-associated enzymes can directly localize to LDs and synthesize TAG at the surfaces of LDs (13–15), which is then incorporated to produce LD growth.

Fusion or coalescence of adjacent LDs can also lead to expanded LDs or giant LDs (gLDs). So far, three main forms of LD fusions have been reported. The first is a slow fusion (often takes around 60 min) of LDs regulated by CIDE (cell death–inducing DNA fragmentation factor alpha–like effector) family proteins that enrich at the LD–LD contact site (16), mediating the directional lipid transfer from a small to a large LD in various tissues including adipose tissues and liver. Second, when the phosphatidylcholine (PC) level is reduced in *Drosophila*, and/or the phosphatidic acid (PA) level is increased in yeast (9, 17, 18), the LDs in close proximity to each other contact and mix their content within seconds. Third, in *Caenorhabditis elegans*, temperature shifting from 20 to 30 °C can induce LD fusion, which happens within 30 s (19). However, the underlying mechanisms for both the PL-mediated and the thermosensitive LD fusion are still unclear. For example, the carbon length or saturation level of

‡ These authors contributed equally to this work.
* For correspondence: Bin Liang, liangb73@ynu.edu.cn; Xiaoju Zou, xiaojuzou@163.com; Yingjie Wu, yjwu@sdfmu.edu.cn.

the fatty acid chain in PA/PC-mediated LD fusion is completely unknown. In addition, it is also unknown whether there are other distinct mechanisms leading to LD fusion/growth.

In cells, the peroxisomes, similar to LDs, regulate lipid and energy metabolism. Peroxisomes and LDs share biogenesis steps (20, 21), and membrane contact sites between LDs and peroxisomes have also been described (22, 23). Mice lacking peroxisome biogenesis genes, such as PEX5 (24), single peroxisomal enzyme deficiencies in ACOX (acyl-CoA oxidase) (25), or multifunctional enzyme type (multifunctional protein) (26), display enlarged LDs in the liver, testis, or retina. Consistently, dysfunction of ACOX homologs (CG4586 and CG9527) in *Drosophila* (27), or PRX-10 and peroxisomal β-oxidation in *C. elegans* (28–30), also leads to the enlarged LDs. These conserved observations across evolutionary organisms demonstrate a connection between peroxisome and LD growth. However, the role of peroxisomes in LD growth/expansion and the underlying mechanism remains largely unknown.

Using the genetically tractable animal model *C. elegans*, we showed that the formation of gLDs in animals with a dysfunction in peroxisomal β-oxidation was actually because of the fusion of adjacent LDs in less than 30 s. Notably, we discovered that n≥3-PUFAs might trigger this rapid fusion process.

Results

Disruption of peroxisomal β-oxidation triggers the rapid fusion of adjacent LDs to form gLDs

Peroxisomes are subcellular organelles that function in multiple anabolic and catabolic processes, in particular the β-oxidation of long-chain fatty acids (LCFAs). In *C. elegans*, similar to other organisms, the peroxisomal β-oxidation cycle involves four steps catalyzed by four distinct enzymes, ACOX, MAOC-1 (enoyl-CoA hydratase), DHS-28 (3-hydroxylacyl-CoA dehydrogenase), and DAF-22 (3-ketoacyl-CoA thiolase) (28, 30, 31) (Fig. 1*A*). Both Nile Red and LipidTOX have been widely used to visualize LDs in fixed *C. elegans* through staining the neutral lipid TAGs and cholesterol esters (32, 33). DHS-3 encodes a short-chain dehydrogenase, which is almost exclusively localized on *C. elegans* LDs. Therefore, DHS-3::GFP {N2, *ldrIs1[Pdhs3::dhs-3::gfp+unc-76(+)]*} is also used as an LD marker in *C. elegans* (33). In the intestine of *C. elegans*, the major site of lipid synthesis and storage, all the aforementioned three methods consistently revealed that the *acox-3(tm4033)*, *maoc-1(hj13)*, *dhs-28(tm2581)*, and *daf-22(ok693)* mutants displayed a few gLDs (5–6% of total LDs larger than 5 μm), which were undetectable in the wildtype N2 worms (Fig. 1, *B* and *C*). These results demonstrate that disruption of any step of the peroxisomal β-oxidation pathway leads to gLDs.

C. elegans contains seven paralogs of ACOXs including ACOX-3 (Fig. S1*A*), which is a close homolog of CG4586 in *Drosophila*, and ACOX1 in mice and humans (Fig. S1*B*) (34, 35). We therefore tested whether other members of the *acox* family also regulated the LD size. Nile Red staining of fixed worms showed that none of the other *acox* mutant worms displayed an altered LD size, with the exception of the *acox-3(tm4033)* mutant worms showing gLDs and the *acox-1.5(ok2619)* mutant worms showing a slightly reduced LD size (Fig. S1, *C* and *D*). Next, to test if the gLDs in the *acox-3(tm4033)* mutant was specifically because of the dysfunction of ACOX-3, we generated a transgenic worm strain *acox-3::gfp* {N2;*unc-119(ed3);kunEx233[Pacox-3::acox-3::gfp]*}. Through GFP fluorescence analysis, ACOX-3::GFP is mainly expressed in the intestine of worms and had no obvious effect on LD size (Fig. S1, *E*–*G*). We then crossed the *acox-3::gfp* strain into the *acox-3(tm4033)* mutant background. As expected, the gLDs completely disappeared in the *acox-3(tm4033);acox-3::gfp* worms compared with the *acox-3(tm4033)* mutant worms (Fig. S1, *F* and *G*), confirming that gLD formation is indeed because of the loss of function of *acox-3*.

The gLDs may originate from the growth of LD *per se* or by the fusion of adjacent LDs (Fig. 1*D*). The gLDs in the worms with a peroxisomal β-oxidation defect display an unevenly/nonasymmetric distribution, which looks comparable to the LD phenotype of the reported *cct-1* mutant in the *Drosophila* S2 cell line (17) and the *fld-1* mutant in yeast (9), in which the adjacent LDs fuse to form a gLD. We therefore hypothesized that the formation of gLDs in worms with a peroxisomal β-oxidation defect may be a result of adjacent LD fusion. Using time-lapse video microscopy on living worms with the LD marker DHS-3::GFP uncovered that two adjacent LDs closed, contacted, and then fused into a gLD in 10 to 30 s in all *acox-3(tm4033)*, *maoc-1(hj13)*, *dhs-28(tm2581)*, and *daf-22(ok693)* mutant worms but not in the wildtype N2 worms (Fig. 1*E*) (Movies S1–S5). In order to avoid the possible unknown role of DHS-3 overexpression on the LD fusion process, we also performed the time-lapse video microscopy on living worms using bright-field mode with differential interference contrast and found the same effects on LD fusion in the peroxisomal β-oxidation defect worms (Fig. 1*F*) (Movies S6–S10). Thus, dysfunction of peroxisomal β-oxidation can trigger LD fusion that leads to gLDs. Since this process of LD fusion is distinctly very fast (less than 30 s), we named this process as the rapid fusion of LDs.

Dysfunction of peroxisomal β-oxidation causes fatty acid-CoA accumulation

C. elegans contains a series of unsaturated fatty acids including n-3 and n-6 polyunsaturated fatty acids (PUFAs), which can be *de novo* synthesized from acetyl-CoA through many steps of elongations and desaturations (31, 36, 37) (Fig. 2*A*). These unsaturated fatty acids, also called LCFAs, can be used as substrates for the biosynthesis of complex lipids or can be broken down into medium-chain fatty acids/short-chain fatty acids (SCFAs) through peroxisomal β-oxidation (Fig. 1*A*). We wondered if dysfunction of peroxisomal β-oxidation might affect fatty acid metabolism. We first examined the fatty acid compositions in these peroxisomal β-oxidation mutants. However, GC analysis did not show a

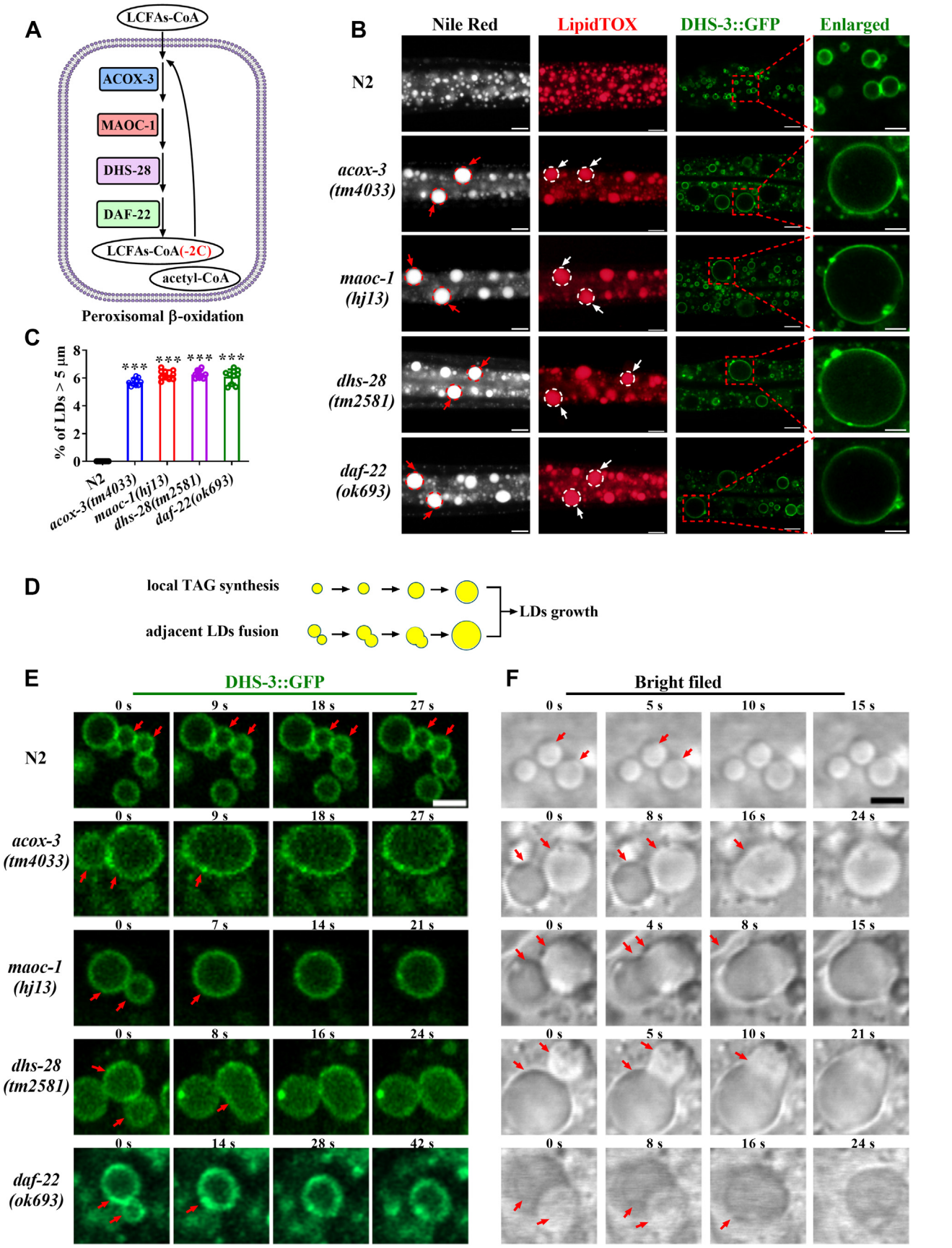

Figure 1. Dysfunction of peroxisomal β-oxidation pathway led to the formation of giant LDs (gLDs) in *Caenorhabditis elegans*. *A*, diagram of fatty acid catabolism by the ACOX-3/MAOC-1/DHS-28/DAF-22 peroxisomal β-oxidation pathway in *C. elegans*. *B*, lipid droplets (LDs) of L4 worms including the wildtype strain N2, *acox-3(tm4033)*, *maoc-1(hj13)*, *dhs-28(tm2581)*, and *daf-22(ok693)* mutants were visualized by postfixed Nile Red staining, postfixed

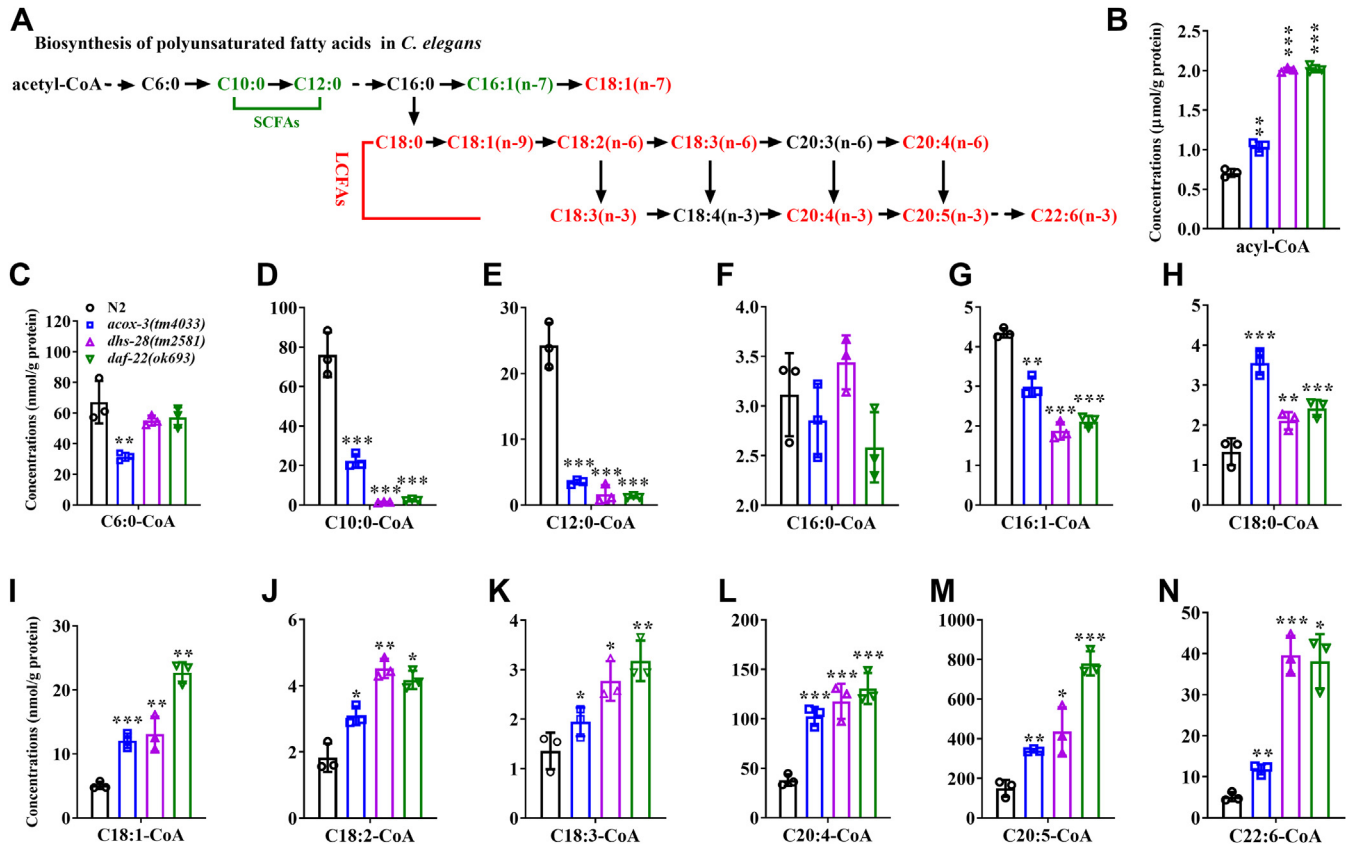

Figure 2. Accumulation of PUFAs-CoA in the peroxisomal β-oxidation defect worms. *A*, diagram of the biosynthesis of PUFAs in *Caenorhabditis elegans*. *B–N*, the levels of acyl-CoA (*B*), C6:0-CoA (*C*), C10:0-CoA (*D*), C12:0-CoA (*E*), C16:0-CoA (*F*), C16:1-CoA (*G*), C18:0-CoA (*H*), C18:1-CoA (*I*), C18:2-CoA (*J*), C18:3-CoA (*K*), C20:4-CoA (*L*), C20:5-CoA (*M*), and C22:6-CoA (*N*), in the wildtype N2, *acox-3(tm4033)*, *dhs-28(tm2581)*, and *daf-22(ok693)* mutants. All data are presented from three independent biological replicates. Significant difference between a specific mutant and wildtype N2, $*p < 0.05$, $**p < 0.01$, and $***p < 0.001$. PUFA, polyunsaturated fatty acid.

significant change of the fatty acid compositions in these mutants compared with the wildtype N2 (Table S1).

In fact, fatty acids must first be activated by acyl-CoA synthase to form fatty acid-CoA in order for anabolism or catabolism to proceed. Therefore, we detected the fatty acids-CoA using LC–MS in these peroxisomal β-oxidation mutants. In total, the level of acyl-CoA was consistently significantly increased in three tested mutant worms, *acox-3(tm4033)*, *dhs-28(tm2581)*, and *daf-22(ok693)*, compared with the wildtype N2 worms (Fig. 2*B*). Of which, the levels of SCFAs-CoAs C10:0-CoA and C12:0-CoA were decreased (Fig. 2, *D* and *E*), whereas the levels of seven LCFAs-CoA including C18:0-CoA, C18:1-CoA, C18:2-CoA, C18:3-CoA, C20:4-CoA, C20:5-CoA, and C22:6-CoA were increased (Fig. 2, *H–N*), in the aforementioned mutant worms. Taken together, these results suggest that the *C. elegans* peroxisomal β-oxidation catalyzes the conversion of LCFAs-CoA to SCFAs-CoA.

Inactivation of PUFA biosynthesis eliminates the gLDs in peroxisomal β-oxidation mutants

As mentioned previously, dysfunction of peroxisomal β-oxidation causes not only gLDs but also altered fatty acid metabolism, raising the question of whether they had a direct connection. The gLDs might be caused by either the reduction of SCFAs-CoA or the accumulation of LC/very long–chain fatty acids-CoA in the peroxisomal β-oxidation mutants. Since the four peroxisomal β-oxidation mutant worms displayed consistent gLDs and altered fatty acids-CoA, we chose the *dhs-28(tm2581)* and *daf-22(ok693)* mutants for most of the following experiments for convenience.

To distinguish both possibilities, we first fed dietary fatty acids C10:0 or C12:0 to *dhs-28(tm2581)* and *daf-22(ok693)* mutant worms. However, dietary supplementation of C10:0 or C12:0 could not repress the gLD formation in these mutant worms (Fig. S2, *A* and *B*), suggesting that the gLDs

LipidTOX staining, and LD marker DHS-3::GFP{N2, *ldrls1[Pdhs-3::dhs-3::gfp+unc-76(+)]*}. For all representative animals, anterior is left and posterior is right. The scale bar represents 10 μm for the first (Nile Red) and second rows (LipidTOX), 5 μm for the third row (DHS-3::GFP), and 2 μm for the fourth row (enlarged). The *dashed circles* and *arrows* indicated the representative giant LDs (gLDs). *C*, percentage (%) of Nile Red-stained LDs with diameters ≥5 μm as quantified from (*B*). Data are presented as mean ± SD. n = 10 for each worm strain. Significant difference between a specific mutant and wildtype N2, $***p < 0.001$. *D*, diagram of LD growth. *E* and *F*, representative fusion events of two adjacent LDs (indicated by *red arrows*) visualized by LD marker DHS-3::GFP under fluorescent light (*E*) and bright field (*F*) in the wildtype N2, *acox-3(tm4033)*, *maoc-1(hj13)*, *dhs-28(tm2581)*, and *daf-22(ok693)* mutant worms. The scale bar represents 2 μm. The *arrows* indicated two adjacent LDs fusing to form gLDs. ACOX-3, acyl-CoA oxidase 3; DAF-22, 3-ketoacyl-CoA thiolase; DHS-28, 3-hydroxylacyl-CoA dehydrogenase; LCFA-CoA, long-chain fatty acid-CoA; MAOC-1, enoyl-CoA hydratase.

might not be caused by the reduction of SCFAs-CoA. In *C. elegans*, the desaturases FAT-1, FAT-2, and FAT-3 are involved in the biosynthesis of PUFAs containing two or more double bonds (Fig. 3*A*) (31, 37). Quantitative PCR (qPCR) analysis revealed that the mRNA levels of *fat-1*, *fat-2*, and *fat-3* were significantly upregulated in both *dhs-28(tm2581)* and *daf-22(ok693)* mutant worms compared with the wildtype N2 worms (Fig. 3*B*), implying an upregulated desaturation of PUFAs in peroxisomal β-oxidation mutants.

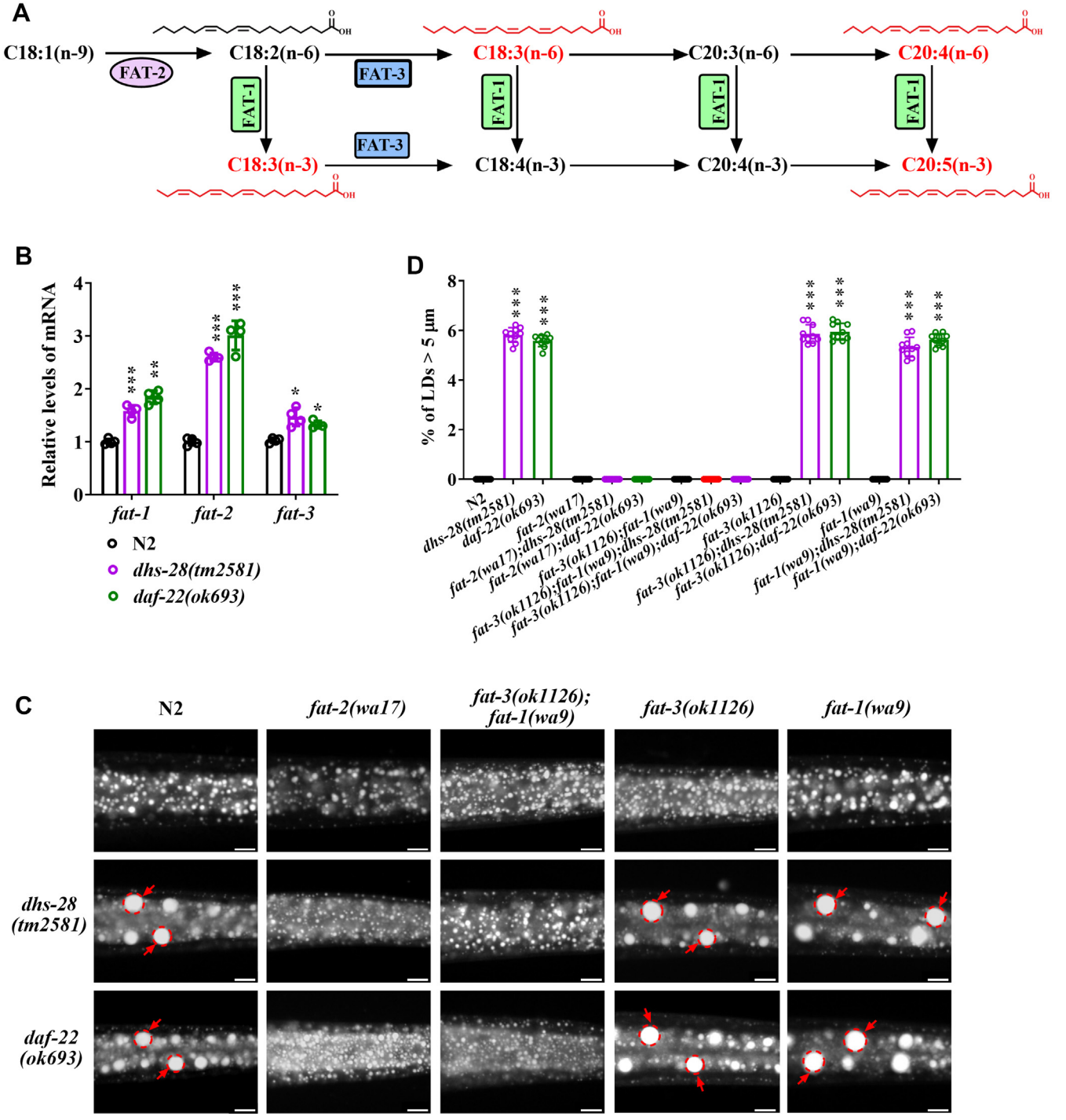

Figure 3. Inactivation of n≥3-PUFAs biosynthesis eliminates gLD formation in peroxisomal β-oxidation defect worms. *A*, diagram of the structure and biosynthesis pathway of PUFAs in *Caenorhabditis elegans*. *B*, the relative mRNA level of *fat-1*, *fat-2*, and *fat-3* in the wildtype N2, *dhs-28(tm2581)*, and *daf-22(ok693)* mutant worms. *C*, Nile Red staining of fixed L4 worms. For all representative animals, anterior is left and posterior is right. The scale bar represents 10 μm. The *dashed circles* and *arrows* indicated representative gLDs. *D*, percentage (%) of gLDs with diameters >5 μm quantified from (*C*). n = 10 for each worm strain. All data are presented from three independent biological replicates. Significant difference between a specific mutant and wildtype N2, $^{*}p < 0.05$, $^{**}p < 0.01$, and $^{***}p < 0.001$. gLD, giant LD; PUFA, polyunsaturated fatty acid.

n≥3-PUFAs promote lipid droplet fusion

To determine which specific LCFA was required for the formation of gLDs, we then crossed *fat-1(wa9)*, *fat-2(wa17)*, and *fat-3(ok1126)* mutants into the *dhs-28(tm2581)* and *daf-22(ok693)* mutants, respectively. Inactivation of FAT-2 results in a loss of all PUFAs (Figs. 3*A*, and S2*C*). As well, the gLDs also disappeared in the *fat-2(wa17);daf-22(ok693)* and *fat-2(wa17);dhs-28(tm2581)* double mutants compared with their corresponding *daf-22(ok693)* and *dhs-28(tm2581)* single mutant, respectively (Fig. 3, *C* and *D*). In addition, the *fat-2(wa17)* mutation also suppressed the gLDs in the *acox-3(tm4033)* and *maoc-1(hj13)* mutant worms (Fig. S2, *D* and *E*). These results indicate that PUFAs are necessary for the formation of gLDs in the peroxisomal β-oxidation mutants.

Inactivation of both FAT-1 and FAT-3 blocks the biosynthesis of PUFAs with three or more double bonds (Figs. 3*A* and S2*C*). Similar to the *fat-2(wa17);daf-22(ok693)* and *fat-2(wa17);dhs-28(tm2581)* double mutants, the *fat-3(ok1126);fat-1(wa9);daf-22(ok693)* or *fat-3(ok1126);fat-1(wa9);dhs-28(tm2581)* triple mutants also had undetectable gLDs (Fig. 3, *C* and *D*), suggesting that PUFAs bearing three or more double bonds (simply named as n≥3-PUFAs), but not C18:2(n-6), are necessary for the formation of gLDs in the peroxisomal β-oxidation mutants. Inactivation of FAT-3 alone blocks the biosynthesis of C18:3(n-6), C18:4(n-3), and their downstream products, C20-PUFAs (Figs. 3*A* and S2*C*). However, the *fat-3(ok1126);daf-22(ok693)* and *fat-3(ok1126);dhs-28(tm2581)* double mutants still had gLDs (Fig. 3, *C* and *D*), which might be due to the presence of C18:3(n-3). Meanwhile, inactivation of FAT-1 impairs the conversion of omega-6 (n-6) PUFAs to omega-3 (n-3) PUFAs (Figs. 3*A* and S2*C*), whereas the *fat-1(wa9);daf-22(ok693)* and *fat-1(wa9);dhs-28(tm2581)* double mutants still displayed gLDs (Fig. 3, *C* and *D*), suggesting that the C18:3(n-6), C20:3(n-6), and C20:4(n-6) in these mutants may still be involved in the formation of gLDs. Altogether, these lines of evidences uncover that n≥3-PUFAs (LCFAs) are necessary for the formation of gLDs in the peroxisomal β-oxidation mutants.

Dietary n≥3-PUFAs are sufficient to promote the formation of gLDs in the peroxisomal β-oxidation mutants

As mentioned previously, the loss of n≥3-PUFAs (LCFAs) by mutations of desaturases could abolish the formation of gLDs in the peroxisomal β-oxidation mutants. We next asked whether supplementation of n≥3-PUFAs could restore the gLDs in these mutants. Since either the *fat-3(ok1126);fat-1(wa9)* double mutations or the *fat-2(wa17)* single mutation could completely abolish the gLDs in the *daf-22(ok693)* and *dhs-28(tm2581)* mutant worms, we therefore tested their response to dietary supplementation of n≥3-PUFAs. We first confirmed the successful uptake of each dietary PUFA by worms using GC (Fig. S3).

Inactivation of FAT-2 blocks the biosynthesis of C18:2(n-6) and its downstream fatty acids (Figs. 3*A* and S2*C*). Dietary C18:2(n-6), C18:3(n-6), C18:3(n-3), C20:4(n-6), and C20:5(n-3) had no effect to promote the formation of gLDs in the wildtype N2, *fat-2(wa17)* single mutant, and *fat-3(ok1126);fat-1(wa9)* double mutant worms (Fig. 4, *A* and *B*). However, remarkably, these dietary fatty acids could fully restore the gLDs in the *fat-2(wa17);daf-22(ok693)* (Fig. 4, *A* and *B*) and *fat-2(wa17);dhs-28(tm2581)* mutant worms (Fig. S4, *A* and *B*), suggesting that PUFAs are essential to promote gLD formation in the peroxisomal β-oxidation mutants. Inactivation of both FAT-1 and FAT-3 impairs the conversion of C18:2(n-6) to n≥3-PUFAs (Figs. 3*A* and S2*C*). Dietary C18:3(n-3), C18:3(n-6), C20:4(n-6), and C20:5(n-3), but not C18:2(n-6), also successfully restored the gLDs in the *fat-3(ok1126);fat-1(wa9);daf-22(ok693)* (Fig. 4, *A* and *B*) and *fat-3(ok1126);fat-1(wa9);dhs-28(tm2581)* (Fig. S4, *A* and *B*) triple mutant worms. Thus, the recovery of the gLDs in the *fat-3(ok1126);fat-1(wa9);daf-22(ok693)* and *fat-3(ok1126);fat-1(wa9);dhs-28(tm2581)* triple mutant worms by individual dietary C18:3(n-3), C18:3(n-6), C20:4(n-6), or C20:5(n-3), but not C18:2(n-6), clearly demonstrates that PUFAs with three or more double bonds are sufficient to trigger the formation of gLDs in the peroxisomal β-oxidation mutants.

n≥3-PUFAs–PC promotes gLD formation in peroxisomal β-oxidation mutants

PUFAs can be incorporated into complex lipids such as TAGs and PLs, including PC, phosphatidylethanolamine (PE), phosphatidylinositol (PI), and phosphatidylserine (PS), which composes the lipids core and the enclosed PL monolayer of LDs, respectively. Since n≥3-PUFAs are required for the formation of gLDs in the peroxisomal β-oxidation mutants, we thereby asked which complex lipid containing n≥3-PUFAs is involved in this process.

To do so, the total lipids (nTL), nTAG, and nPL (containing 50 μg fatty acids), which contains n≥3-PUFAs in different degrees, were isolated from the wildtype N2 worms ("n" stands for lipids isolated from N2) and then were individually added to the nematode growth media (NGM) plates and cultured with different worm strains. The isolated complex lipids with PUFAs were confirmed using GC (Fig. 5*A*). Supplementation of nTL, nTAG, and nPL, similar to dietary PUFAs (Fig. 4, *A* and *B*), did not cause any effect on the LD phenotypes of the N2, *daf-22(ok693), fat-3(ok1126);fat-1(wa9)* worms. However, supplementation of nTL and nPL completely reproduced the gLDs in the *fat-3(ok1126);fat-1(wa9);daf-22(ok693)* mutant worms (Fig. 5, *A* and *B*). In addition, nTAG, which also contains a very small amount of C20-PUFAs such as 20:4(n-3) and 20:5(n-3) (31), had the same effect but to a much lesser degree for the formation of gLDs (Fig. 5, *A* and *B*).

The PLs are divided into several distinct molecular classes, distinguished by the head group attached to the phosphate moiety, such as PC, PE, PI, and PS. To determine which PL type is involved in the formation of gLDs, we further extracted and separated *C. elegans* nPC, nPE, nPI, and nPS and then individually added them to different worm strains. We used the commercial standard sPC, sPE, sPI, and sPS as their corresponding controls ("s" is standard for commercial lipids). Very consistently, similar to applying nPL, applying nPC and sPC, which contains a small amount of C20:4(n-6) (Fig. 5, *A* and *B*), could successfully trigger the formation of the gLDs in the *fat-3(ok1126);fat-1(wa9);daf-22(ok693)* mutant worms (Fig. 5, *A*

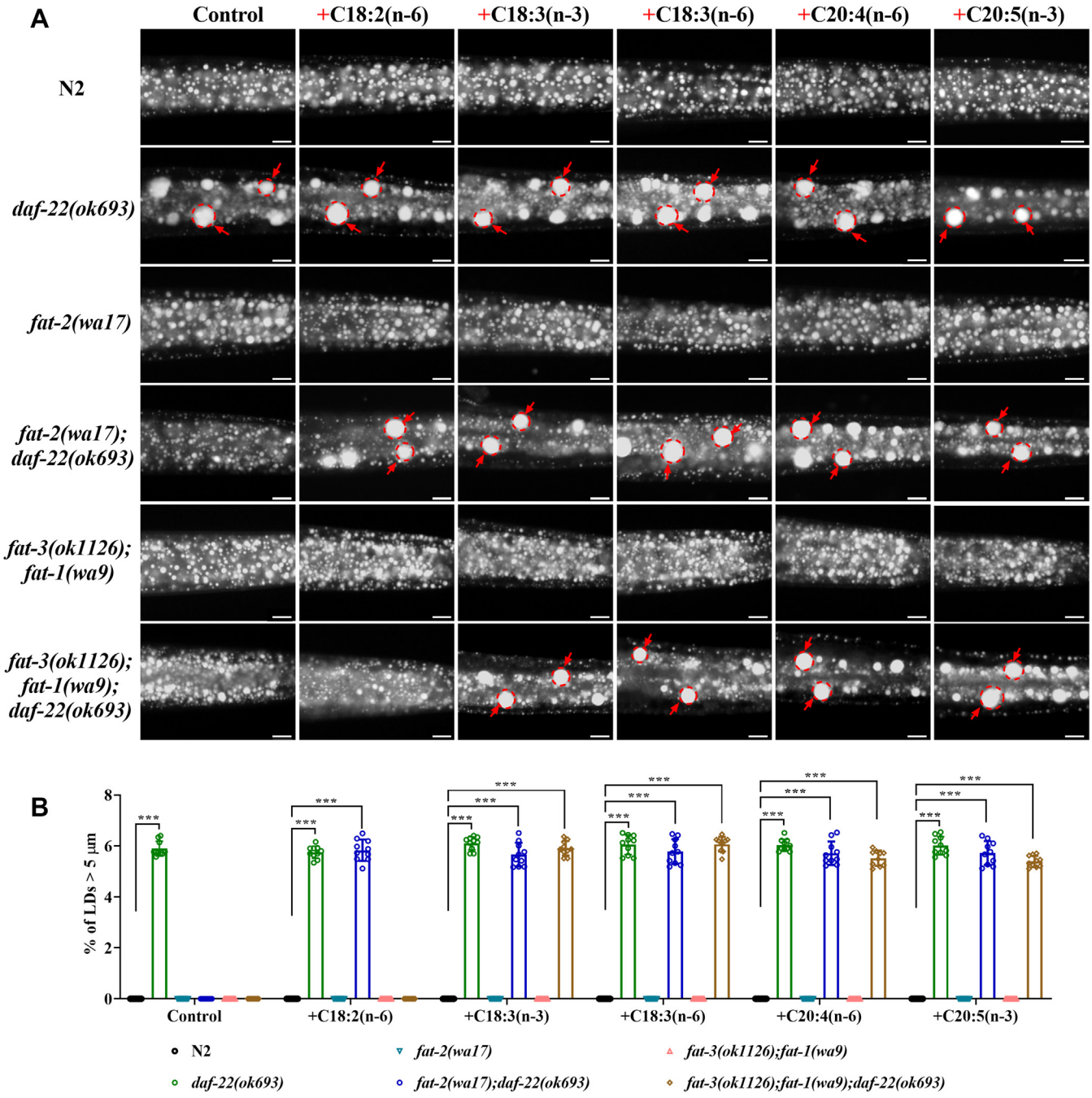

Figure 4. Dietary n≥3-PUFAs recover gLD formation in peroxisomal β-oxidation defect worms without PUFA biosynthesis. *A*, Nile Red staining of fixed L4 worms. For all representative animals, anterior is left and posterior is right. The scale bar represents 10 μm. The *dashed circles* and *arrows* indicated representative gLDs. "+" indicated the supplementation of a specific fatty acid. *B*, percentage (%) of LDs with diameters >5 μm as quantified from (*A*). n = 10 for each worm strain. All data are presented from three independent biological replicates. Significant difference between a specific mutant and wildtype N2 under same treatment, ***$p < 0.001$. gLD, giant LD; PUFA, polyunsaturated fatty acid.

and *B*). In contrast, supplementation of *f*PC, which was isolated from *fat-3(ok1126);fat-1(wa9)* mutant worms that completely lack n≥3-PUFAs, or commercial 16:0-PC bearing C16:0 at the *sn-1* and *sn-2* positions of PC, failed to produce gLDs in the *fat-3(ok1126);fat-1(wa9);daf-22(ok693)* mutant worms (Fig. 5, *A* and *B*). Meanwhile, the levels of total PC and PC bearing UFAs containing one or more double bonds were significantly increased in the *daf-22(ok693)* and *dhs-28(tm2581)* mutant worms compared with the wildtype N2 worms (Fig. 5, *C*–*F*). On the other hand, surprisingly, although the nPE, nPI, and nPS contain n≥3-PUFAs, they could not recover the gLDs in the *fat-3(ok1126);fat-1(wa9);daf-22(ok693)* mutant worms (Fig. S5, *A* and *B*). Moreover, the dietary sPE, sPI, and sPS, which lack PUFAs, also had no effect to trigger gLD formation in the *fat-3(ok1126);fat-1(wa9);daf-22(ok693)* mutants (Fig. S5, *A* and *B*). Altogether, these lines of evidences suggest that the choline

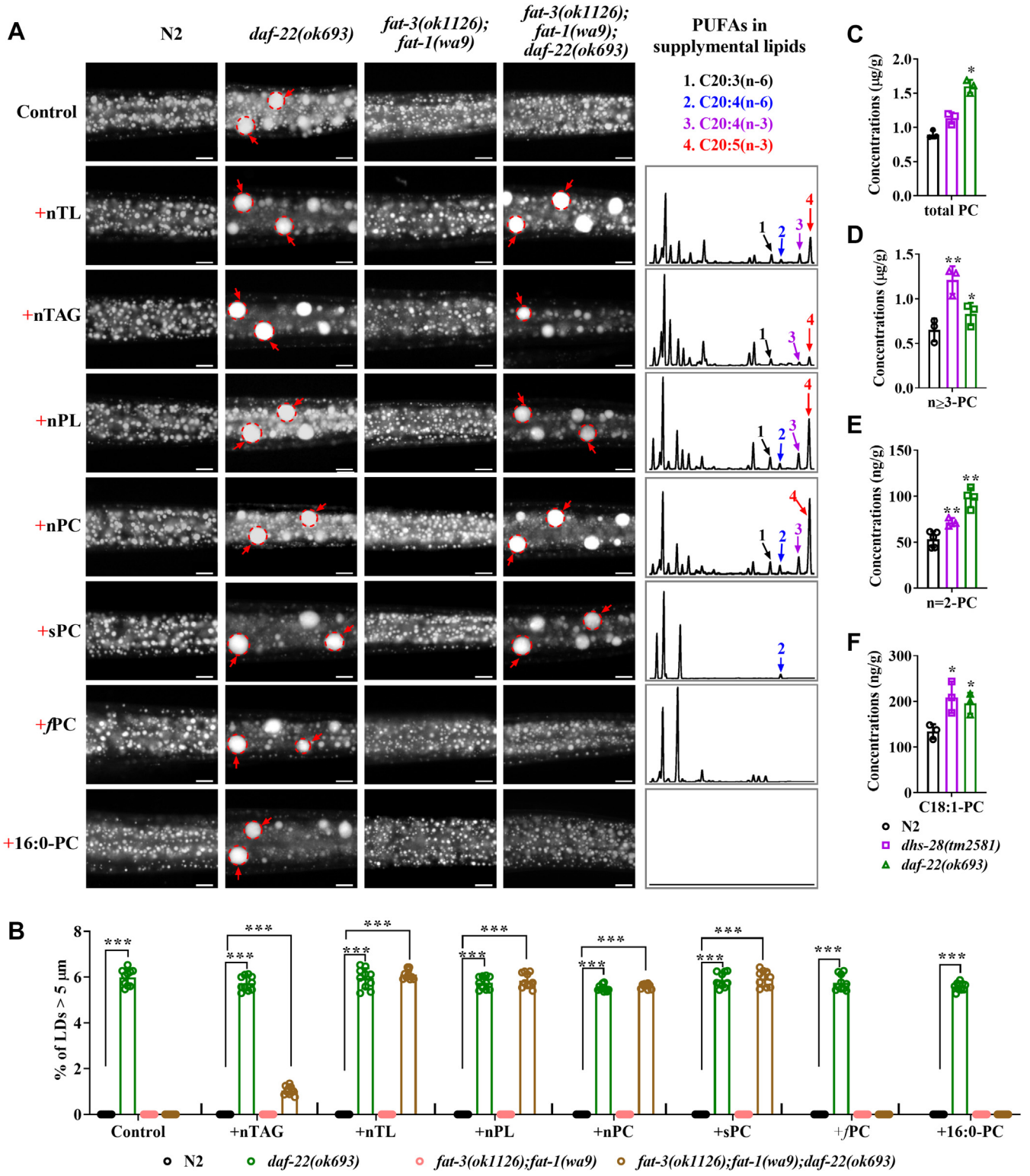

Figure 5. n≥3-PUFA-PC determines the gLD formation. *A*, *left panel*, Nile Red staining of fixed L4 worms supplemented with different lipid species. "n" represents lipids isolated from N2 worms. "s" represents standard commercial PL purchased from Sigma. "*f*" represents lipid isolated from the *fat-3(ok1126);fat-1(wa9)* worms. For all representative animals, anterior is left and posterior is right. The scale bar represents 10 μm. The *dashed circles* and *arrows* indicated the representative gLDs. The *right panel* showed the GC profile of PUFAs in different lipid species supplemented to worms. "1" indicates C20:3(n-6), "2" indicates C20:4(n-6), "3" indicates C20:4(n-3), and "4" indicates C20:5(n-3). *B*, percentage (%) of LDs with diameters >5 μm as quantified from (*A*). n = 10 for each worm strain. *C–F*, the levels of total PC (*C*), n≥3 PC with three or more double bonds on the sn-2 position (*D*), n = 2 PC with two double bonds (n = 2) on the sn-2 position (*E*), C18:1 PC with C18:1 on the sn-1 and/or sn-2 position (*F*) in worms. All data are presented from three independent biological replicates. Significant difference between a specific mutant and wildtype N2 under same treatment, *$p < 0.05$, **$p < 0.01$, and ***$p < 0.001$. gLD, giant lipid droplet; PC, phosphatidylcholine; PL, phospholipid; PUFA, polyunsaturated fatty acid.

headgroup and n≥3-PUFAs as fatty acid chain are two indispensable factors for PC to promote gLD formation in the peroxisomal β-oxidation mutants.

Dysfunction of peroxisomal β-oxidation activates sterol regulatory element–binding protein to promote gLD formation

The sterol regulatory element–binding proteins (SREBPs) play important roles regulating lipid homeostasis from *C. elegans* to mammals (31, 38). The sterol-binding protein 1 (SBP-1), a homolog of mammalian SREBP-1, has been reported to regulate fatty acid and PL biosynthesis in *C. elegans* (39–42). A previous report showed that blocking SAMe or PC synthesis in *C. elegans,* mouse liver, and human cells activates SREBP-1 to promote LD accumulation (40). We thereby asked whether dysfunction of peroxisomal β-oxidation, which leads to the accumulation of fatty acids-CoA and PC, could also regulate SREBP-1 to trigger gLD formation.

qPCR analysis showed that the mRNA expression of *sbp-1* was significantly increased in *daf-22(ok693)* and *acox-3(tm4033)* mutant worms compared with the wildtype (N2) worms (Fig. 6*A*). In addition, we crossed the *gfp::sbp-1* {N2;*ftIs7(Psbp-1::gfp::sbp-1)*} strain into *daf-22(ok693)* and *acox-3(tm4033)* mutants and found that the fluorescence intensity of GFP::SBP-1 was consistently upregulated in nuclear but downregulated in cytosol in *daf-22(ok693)* and *acox-3(tm4033)* mutant worms (Fig. 6, *B* and *C*), suggesting an activated SBP-1 when the peroxisomal β-oxidation is disrupted. Next, to test whether SBP-1 was necessary for gLD formation, we crossed *sbp-1(ep79)* mutant into *daf-22(ok693)* and *acox-3(tm4033)* mutant to generate *sbp-1(ep79);daf-22(ok693)* and *sbp-1(ep79);acox-3(tm4033)* double mutant worms. Although the mRNA expression of *fat-1*, *fat-2*, and *fat-3* was significantly increased in both *daf-22(ok693)* and *acox-3(tm4033)* mutant worms, inactivation of SBP-1 (*ep79* mutation) could abolish these effects (Fig. 6*A*). More importantly, the gLDs disappeared in *sbp-1(ep79);daf-22(ok693)* and *sbp-1(ep79);acox-3(tm4033)* double mutant worms compared with the *daf-22(ok693)* or *acox-3(tm4033)* single mutant worms, respectively (Fig. 6, *D* and *E*), suggesting that the gLD formation depends on the activity of SBP-1. Collectively, these results demonstrate that peroxisomal β-oxidation dysfunction activates SBP-1 to promote gLD formation.

Discussion

LDs are dynamic organelles whose number and size undergo constant changes in response to internal and external energy demands (43). Previous studies have reported that the LD fusion can be mediated by CIDE family proteins, taking around an hour, as well as reduction of PC (18) in *Drosophila* (17), or an increase of PA in yeast within a minute (9). The *C. elegans* peroxisomal β-oxidation pathway consists of four enzymes: ACOX-3, MAOC-1, DHS-28, and DAF-22 to break down the LCFAs. In this study, we found that inactivation of this process leads to a few gLDs, which are actually formed by the fusion of adjacent LDs within 30 s. Furthermore, we revealed that inactivation of peroxisomal β-oxidation consequently led to the accumulation of n≥3-PUFAs-CoA, which may be incorporated into PC to mediate this rapid fusion process. Thus, we discovered a completely distinct type of rapid LD fusion because of inactivation of peroxisomal β-oxidation in the model organism *C. elegans*.

In *C. elegans*, the peroxisomal β-oxidation pathway was previously reported to catalyze the β-oxidation of LCFAs (30). However, the levels of LCFAs were not changed in the peroxisomal β-oxidation mutants compared with the wildtype N2, which is consistent to a previous report (30). In fact, fatty acids must be activated by acyl-CoA synthase to form fatty acid-CoA in order for anabolism or catabolism to occur. Our data showed that the levels of LCFAs-CoA but not LCFAs were indeed significantly increased, while reversely, the levels of SCFAs-CoA were significantly decreased in the peroxisomal β-oxidation mutants. Therefore, our work uncovers that peroxisomal β-oxidation actually breaks down the LCFAs-CoA, instead of LCFAs, confirming this biological function of LCFAs-CoA β-oxidation in the peroxisome in *C. elegans*.

As the structural lipids in eukaryotic membranes, PLs mainly contain PC, PE, PS, PI, and PA. The PC amount is greater than 50% of all PLs (44) and is the major PL in *C. elegans* (31, 45, 46). PC is cylindrical in shape and provides excellent coverage of the surface area and lower surface tension. Therefore, PC is considered crucially important for LD stability (47). Dysfunction of key synthesis enzyme CCT-1 of PC in *Drosophila* S2 cells (17) or artificial droplets generated *in vitro* with low PC (18) leads to gLDs or to LD coalescence *via* a fusion process. Independent from these findings and on the other hand, we reveal that excessive accumulation of specific PC species may also be involved in LD fusion to form gLDs in the peroxisomal β-oxidation defect mutants in *C. elegans*. Thus, these findings, including our current study, consistently reinforce the idea that the PC regulates LD fusion, because of either its deficiency or accumulation in distinct animal or cell models.

PC commonly involves one cis-unsaturated acyl chain, for instance eicosapentaenoic acid C20:5(n-3), an abundant fatty acid in *C. elegans*. Five cis-double bonds create a strong kink that decreases the packing compactness of the acyl chains and in turn raises membrane fluidity (48). This may influence membrane curvature and fusion events. Peroxisomal biogenesis disorders and peroxisomal β-oxidation defects (PEX13, PEX16, and ACOX1) showed elevated levels of PC species with very long–chain FAs in fibroblasts from patients (49, 50). Very consistently, our in-depth analysis of lipids revealed that inactivation of peroxisomal β-oxidation promoted the accumulation of both LCFAs-CoA, total PC, and PC containing LCFAs in *C. elegans*. In the peroxisomal β-oxidation defect mutants, inactivation of n≥3-PUFAs biosynthesis by inactivation of both FAT-1 and FAT-3 blocked the formation of gLDs, which could be rescued by supplementation of PC only with n≥3-PUFAs (n≥3-PUFAs-PC) but not PC without PUFAs, either isolated from *C. elegans* or by using commercially available products. In addition, feeding other PLs such as PE, PS, PI with or without n≥3-PUFAs had no such an effect. Thus,

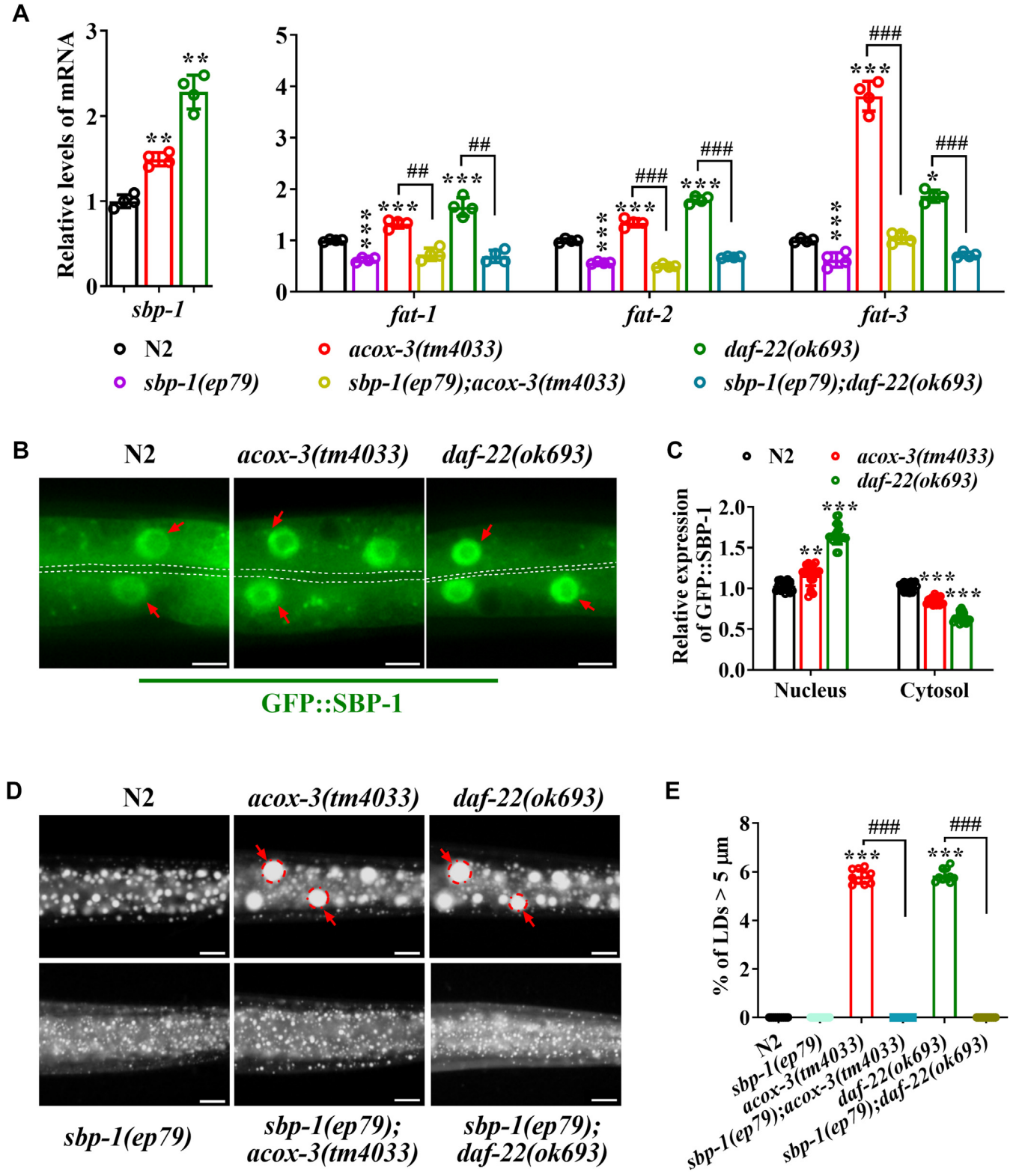

Figure 6. Dysfunction of peroxisomal β-oxidation activates the transcriptional factor SREBP/SBP-1 to promote gLD formation. *A*, the relative mRNA level of *sbp-1*, *fat-1*, *fat-2*, and *fat-3* in different worm strains. *B*, the fluorescence intensity of nuclear and cytosolic GFP::SBP-1 {N2;*ftIs7(Psbp-1::gfp::sbp-1)*} in different worm strains. The scale bar represents 10 μm. *C*, quantification of the fluorescence intensity of nucleus and cytosol GFP::SBP-1 in different worm strains from (*B*). *D*, Nile Red staining of fixed L4 worms. For all representative animals, anterior is left and posterior is right. The scale bar represents 10 μm. The *dashed circles* and *arrows* indicated representative gLDs. *E*, percentage (%) of LDs with diameters >5 μm as quantified from (*D*). n = 10 for each worm strain. All data are presented from three independent biological replicates. Significant difference between a specific mutant and wildtype N2, $^{*}p < 0.05$, $^{**}p < 0.01$, and $^{***}p < 0.001$. Significant difference between two indicated worm strains, $^{\#\#}p < 0.01$, $^{\#\#\#}p < 0.001$. gLD, giant lipid droplet; SBP-1, sterol-binding protein 1; SREBP, sterol regulatory element–binding protein.

we uncovered that it is actually some specific PC species bearing n≥3-PUFAs, but not the general PC, that promotes the rapid LD fusion process. Whether n≥3-PUFAs and n≥3-PUFAs-PC functioning as signal or the membrane constitute of LDs for gLD formation needs future investigation.

The transcription factor SREBP play critical roles to transcriptionally regulate genes involved in fatty acids, triglycerides, and cholesterol metabolism from *C. elegans* to mammals. Previously, we revealed a zinc-mediated regulation of the SREBP-SCD (stearoyl-CoA desaturase) axis in lipid metabolism in *C. elegans* (51). Our current work showed that dysfunction of peroxisomal β-oxidation leads to accumulation of PUFA-CoA and PC, which may activate the nuclear translocation of SREBP to promote gLD formation, distinguishing from the negative regulation of SREBP by PC in *C. elegans* (40). In the peroxisomal β-oxidation defect mutants, whether increased fatty acids-CoA or PCs (or a specific lipid species) activate SREBP directly or *via* another unknown factor and how activated SREBP thereby regulates gLD formation through its transcriptional activity or unknown function needs to be further investigated.

In summary, we propose a model to explain our current work. Inactivation of peroxisomal β-oxidation leads to the accumulation of n≥3-PUFAs-CoA, which in turn, may be incorporated into the PC to promote the rapid fusion of LDs, consequently resulting in gLD formation (Fig. 7).

Experimental procedures

Nematode strains

Worm strains used in this study are listed in Table S2. N2 Bristol was used as the wildtype strain. *C. elegans* worm strains were grown on NGM plates seeded with *Escherichia coli* OP50. All experiments were conducted at 20 °C. All experiments were conducted on NGM plates containing *E. coli* OP50 (CGC) as the food source. A single clone of *E. coli* OP50 was inoculated into LB broth and cultured at 37 °C overnight to stationary phase. Then *E. coli* was seeded directly onto NGM plates. After 24 h drying, the plates were ready for feeding worms.

Construction of transgenic strains

The transgenic strains were created by microinjection following the methods previously described (51). For construction of plasmid *Pacox-3::acox-3::gfp*, the *acox-3* gene of *C. elegans*, including its own 2.845 kb promoter sequence, was

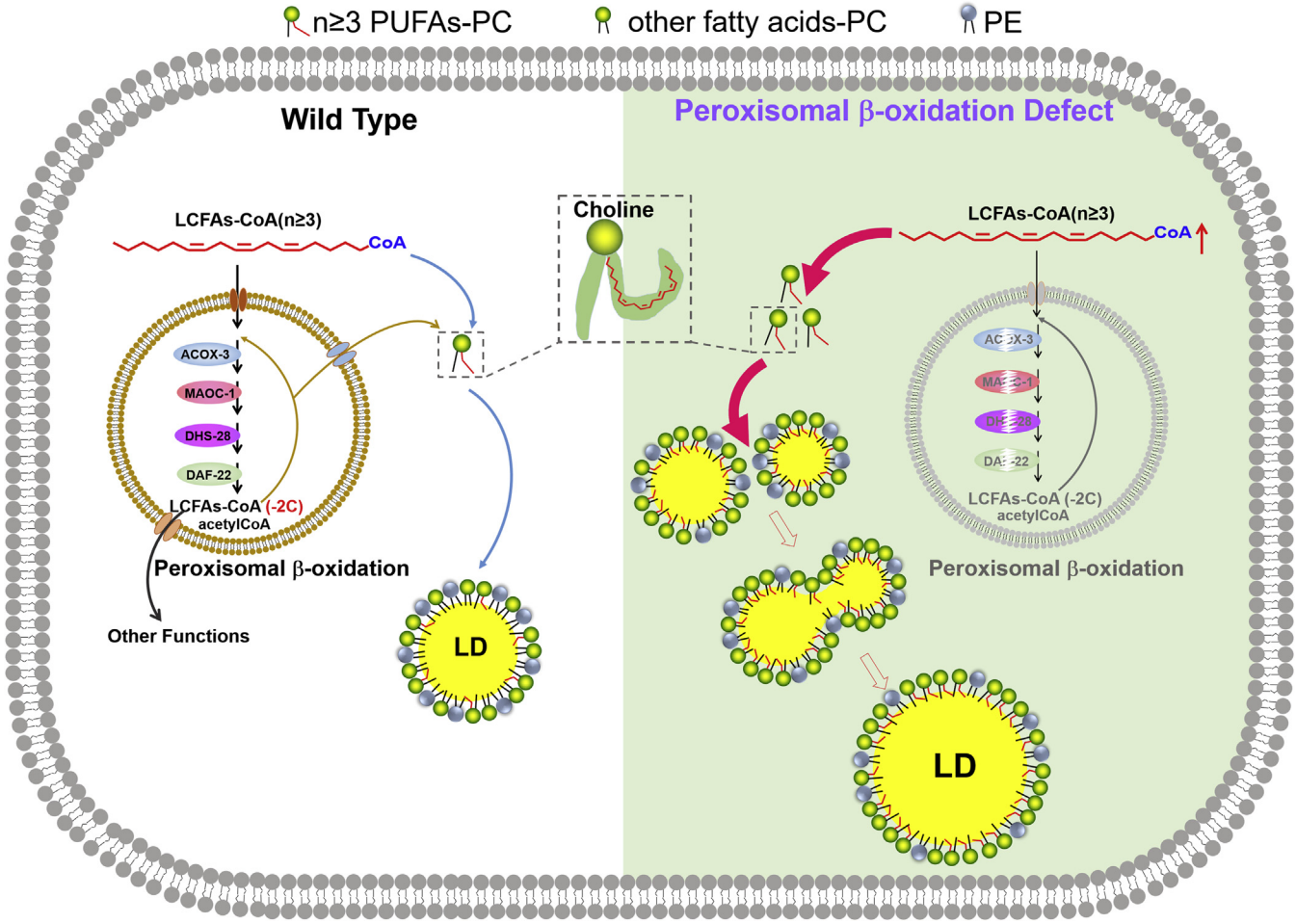

Figure 7. Proposed model. Inactivation of peroxisomal β-oxidation leads to the accumulation of n≥3-PUFAs-CoA, which in turn, may be incorporated into the PC to promote the rapid fusion of LDs, consequently resulting in gLD formation. gLD, giant LD; LD, lipid droplet; PC, phosphatidylcholine; PUFA, polyunsaturated fatty acid.

cloned by PCR. The GFP fragment was amplified from the *pPD95.75* vector. Meanwhile, the vector *pCFJ151* was also fragmented for use. The fragments of *Pacox-3::acox-3* and *gfp* were recombined into the *pCFJ151* vector to generate transgenic plasmids. The primers used for construction of transgenes are listed in Table S3. Approximately 50 ng/μl transgenic plasmids, 50 ng/μl *pJL43.1*, and 3 ng/μl *pCFJ90* were injected into the gonad of EG4322 *[ttTi5605;unc-119(ed3)]*, and progenies expressing GFP were selected (52).

Fatty acid supplementation

Fatty acids were purchased from Nuk Prep, Inc. Individual fatty acid was mixed with bacteria in LB at a concentration of 1 mM. Then, 400 μl of the mixed bacteria were seeded onto the NGM plates (6 cm in diameter). Standard PLs, including sPC, sPE, sPI, and sPS, as well as lipids isolated from *C. elegans* N2 worms including nTAG, nPL (PLs), nTL (total lipids), nPC, nPE, nPI, and nPS, each of these lipids containing equal amount of fatty acids (50 μg) for normalization, were mixed with bacteria and seeded on NGM plates. Synchronized L1 worms were transferred to the NGM plate seeded with *E. coli* and fatty acid/TAG/PL. The worms were harvested at the L4 stage and used for Nile Red staining and GC analysis.

Staining of LDs

Nile Red and LipidTOX were used as the fluorescent dye for staining of neutral fat. Staining of fixed L4 worms was performed as previously described (32, 53). Images of Nile Red staining were used to measure the diameter of the LDs in the posterior of the intestine with the same area (80 μm × 60 μm) using cellSens Standard software (Olympus). For each worm strain with or without treatment, at least three biological repeats were performed and more than 60 worms were observed, 10 representative worms were picked for the quantitation of LD size (diameters).

Lipid extraction, separation, and analysis

Worm lipid extraction, separation, and analysis were performed as previously reported (53). In general, about 200,000 L4 worms were collected, and the protein was quantified with a Pierce BCA Protein Assay Kit. About 15 mg protein was used for total lipid extraction. For lipid separation, 40 μl of total lipid was loaded in triplicate on TLC silica plates (Merck) to separate TAG, PE, PI, PS, and PC. The TLC plates were developed in the solvent system chloroform:ethanol:water:-triethylamine (30:35:7:35) (54) and dried in fume hood. About 0.005% primuline was sprayed evenly on the plate. The spots corresponding to TAG, PE, PI, PS, and PC were visualized under UV light and scraped from TLC plates and transesterified (2.5% H_2SO_4 in methanol). Next, esterified C15:0 was added as an internal standard, and lipids were extracted for GC analysis to determine the relative levels of TAG and PL fractions as previously described (45). Fatty acids were determined with an Agilent 7890 series gas chromatographer equipped with a 30 m × 0.25 mm × 0.25 μm DBWAX column (Agilent), with nitrogen as the carrier gas at 1.4 ml/min, and a flame ionization detector (53).

Analysis of acyl-CoAs

Extraction of acyl-CoAs was carried out as previously described with some modifications (55). Briefly, 300 μl of extraction buffer containing isopropanol, 50 mM KH_2PO_4, and 50 mg/ml bovine serum albumin (25:25:1) acidified with glacial acetic acid was added to the worms. Next, 19:0-CoA was added as an internal standard, and lipids were extracted. To the remaining extracted sample, 5 μl of saturated ammonium sulfate was added followed by 600 μl of chloroform:methanol (1:2). The sample was then incubated on a thermomixer at 450 rpm for 20 min at 25 °C, followed by centrifugation at 12,000 rpm for 5 min at 4 °C. Clean supernatant was transferred to a fresh tube and subsequently dried in a SpeedVac under OH mode (Genevac). Dry extracts were resuspended in an appropriate volume of methanol:water (9:1) prior to LC–MS analyses on a Thermo Fisher U3000 DGLC coupled to Sciex QTRAP 6500 Plus.

Visualization of GFP

L4 worms with GFP markers were washed from NGM plates and settled down in 1.5 ml tubes. The worms were then pipetted and plated onto an agarose gel (2%). Worms were visualized using an Olympus BX53 fluorescence microscope or ZEISS M2 (Zeiss). Images were captured using the same settings and exposure times for each worm, unless specifically indicated, and were analyzed by the CellSens or Zen 2 software.

Confocal microscopy

The LD labeled by DHS-3::GFP was acquired on a confocal microscope LSM880 (Zeiss). For detection of the size of LD, worms with DHS-3::GFP were anesthetized in 1% sodium azide on 2% agarose pads sandwiched between glass microscopic slides and coverslips. About 30 worms of each strain were observed and scored, and the experiment was conducted in three biological replicates. For detection of the LD fusion process, worms were anesthetized in 1 mM levamisole on the lower lid of confocal petri dishes. Then the worms were then covered with 2% agarose and used for microscopy observation. The process of LD fusion was acquired in a λ mode using a 63×, numerical aperture 1.43, with 100 intervals. A z-stack of 7 to 9 sections with 0.5 μm in depth was taken for each animal.

mRNA isolation and qPCR

mRNA of L4 worms was isolated as previously described (56). Complementary DNA was synthesized using the PrimeScript RT reagent kit. mRNA levels of each sample were quantified in three biological replicates using SYBR green fluorescence on a real-time PCR instrument 7900HT (ABI). The relative abundance of mRNA transcripts was determined using the ΔΔCt method, and *tbb-2* was used as a reference gene. The primers used for construction of transgene qPCR are listed in Table S3.

Quantification and statistical analysis

All experiments were conducted with at least three or four biological replicates. Data were analyzed using the SPSS software (SPSS, Inc), and presented as the means ± SD, unless specifically indicated. The one-way ANOVA statistical analysis was performed for the significant difference among the control group and experimental groups, and statistical analysis by Student's *t* tests was used for comparison between the means of two groups. All figures were generated using GraphPad Prism 8 (GraphPad Software, Inc) and Photoshop CS6.

Data availability

All data are contained within the article and supporting information.

Supporting information—This article contains supporting information.

Acknowledgments—We thank members of the C. L. Yang and M. T. Pu at Yunnan University for technical assistance and Metabo-Profile Biotechnology Co, Ltd for lipid analysis. This work was supported by the National Natural Science Foundation of China (grant nos.: 32160155, 31860323, 32071281, 32000818, 31600963, 91857113, U1702288, and 31801001), Ministry of Science and Technology of the People's Republic of China (grant nos.: 2018YFA0800700 and 2018YFA0800703), the Yunnan Applied Basic Research Projects (grant nos.: 2019FB048, 2019FB046, 2019FY003021, and 202101AT070009), and grant 2017KF004 from State Key Laboratory for Conservation and Utilization of Bio-Resources in Yunnan, Yunnan University.

Author contributions—Yan. W., X. Z., and B. L. conceptualization; Yan. W, X. Z., and B. L. methodology; Yan. W., Chu. L., and J. Z. formal analysis; Yan. W, Chu. L., J. Z., M. W., Che. L., and Yin. W. investigation; J. X., X. X., L. F., Y. H., and H. Z. resources; Yin. W and B. L. writing–original draft; Yin. W. writing–review & editing; Yan. W. and B. L. supervision.

Conflict of interest—The authors declare that they have no conflicts of interest with the contents of this article.

Abbreviations—The abbreviations used are: ACOX, acyl-CoA oxidase; DAF-22, 3-ketoacyl-CoA thiolase; DHS-28, 3-hydroxylacyl-CoA dehydrogenase; ER, endoplasmic reticulum; gLD, giant LD; LCFA, long-chain fatty acid; LD, lipid droplet; MAOC-1, enoyl-CoA hydratase; NGM, nematode growth media; PA, phosphatidic acid; PC, phosphatidylcholine; PE, phosphatidylethanolamine; PI, phosphatidylinositol; PL, phospholipid; PS, phosphatidylserine; PUFA, polyunsaturated fatty acid; qPCR, quantitative PCR; SBP-1, sterol-binding protein 1; SCFA, short-chain fatty acid; SREBP, sterol regulatory element–binding protein; TAG, triacylglycerol.

References

1. Ohsaki, Y., Cheng, J., Suzuki, M., Shinohara, Y., Fujita, A., and Fujimoto, T. (2009) Biogenesis of cytoplasmic lipid droplets: from the lipid ester globule in the membrane to the visible structure. *Biochim. Biophys. Acta* **1791**, 399–407
2. Olzmann, J. A., and Carvalho, P. (2019) Dynamics and functions of lipid droplets. *Nat. Rev. Mol. Cell Biol.* **20**, 137–155
3. Yang, L., Ding, Y., Chen, Y., Zhang, S., Huo, C., Wang, Y., *et al.* (2012) The proteomics of lipid droplets: structure, dynamics, and functions of the organelle conserved from bacteria to humans. *J. Lipid Res.* **53**, 1245–1253
4. Walther, T. C., Chung, J., and Farese, R. V., Jr. (2017) Lipid droplet biogenesis. *Annu. Rev. Cell Dev. Biol.* **33**, 491–510
5. Chen, F. J., Yin, Y., Chua, B. T., and Li, P. (2020) CIDE family proteins control lipid homeostasis and the development of metabolic diseases. *Traffic* **21**, 94–105
6. Choudhary, V., Ojha, N., Golden, A., and Prinz, W. A. (2015) A conserved family of proteins facilitates nascent lipid droplet budding from the ER. *J. Cell Biol.* **211**, 261–271
7. Murphy, D. J., and Vance, J. (1999) Mechanisms of lipid-body formation. *Trends Biochem. Sci.* **24**, 109–115
8. Wilfling, F., Haas, J. T., Walther, T. C., and Farese, R. V., Jr. (2014) Lipid droplet biogenesis. *Curr. Opin. Cell Biol.* **29**, 39–45
9. Fei, W., Shui, G., Gaeta, B., Du, X., Kuerschner, L., Li, P., *et al.* (2008) Fld1p, a functional homologue of human seipin, regulates the size of lipid droplets in yeast. *J. Cell Biol.* **180**, 473–482
10. Gross, D. A., Zhan, C. Y., and Silver, D. L. (2011) Direct binding of triglyceride to fat storage-inducing transmembrane proteins 1 and 2 is important for lipid droplet formation. *Proc. Natl. Acad. Sci. U. S. A.* **108**, 19581–19586
11. Jacquier, N., Choudhary, V., Mari, M., Toulmay, A., Reggiori, F., and Schneiter, R. (2011) Lipid droplets are functionally connected to the endoplasmic reticulum in *Saccharomyces cerevisiae*. *J. Cell Sci.* **124**, 2424–2437
12. Wang, H., Jiang, X., Wu, J., Zhang, L., Huang, J., Zhang, Y., *et al.* (2016) Iron overload coordinately promotes ferritin expression and fat accumulation in *Caenorhabditis elegans*. *Genetics* **203**, 241–253
13. Fujimoto, Y., Itabe, H., Kinoshita, T., Homma, K. J., Onoduka, J., Mori, M., *et al.* (2007) Involvement of ACSL in local synthesis of neutral lipids in cytoplasmic lipid droplets in human hepatocyte HuH7. *J. Lipid Res.* **48**, 1280–1292
14. Kuerschner, L., Moessinger, C., and Thiele, C. (2008) Imaging of lipid biosynthesis: how a neutral lipid enters lipid droplets. *Traffic* **9**, 338–352
15. Wilfling, F., Wang, H., Haas, J. T., Krahmer, N., Gould, T. J., Uchida, A., *et al.* (2013) Triacylglycerol synthesis enzymes mediate lipid droplet growth by relocalizing from the ER to lipid droplets. *Dev. Cell* **24**, 384–399
16. Gong, J. Y., Sun, Z. Q., Wu, L. Z., Xu, W. Y., Schieber, N., Xu, D. J., *et al.* (2011) Fsp27 promotes lipid droplet growth by lipid exchange and transfer at lipid droplet contact sites. *J. Cell Biol.* **195**, 953–963
17. Guo, Y., Walther, T. C., Rao, M., Stuurman, N., Goshima, G., Terayama, K., *et al.* (2008) Functional genomic screen reveals genes involved in lipid-droplet formation and utilization. *Nature* **453**, 657–661
18. Krahmer, N., Guo, Y., Wilfling, F., Hilger, M., Lingrell, S., Heger, K., *et al.* (2011) Phosphatidylcholine synthesis for lipid droplet expansion is mediated by localized activation of CTP:phosphocholine cytidylyltransferase. *Cell Metab* **14**, 504–515
19. Li, S., Li, Q., Kong, Y., Wu, S., Cui, Q., Zhang, M., *et al.* (2017) Specific regulation of thermosensitive lipid droplet fusion by a nuclear hormone receptor pathway. *Proc. Natl. Acad. Sci. U. S. A.* **114**, 8841–8846
20. Joshi, A. S., Nebenfuehr, B., Choudhary, V., Satpute-Krishnan, P., Levine, T. P., Golden, A., *et al.* (2018) Lipid droplet and peroxisome biogenesis occur at the same ER subdomains. *Nat. Commun.* **9**, 2940
21. Wang, S., Idrissi, F. Z., Hermansson, M., Grippa, A., Ejsing, C. S., and Carvalho, P. (2018) Seipin and the membrane-shaping protein Pex30 cooperate in organelle budding from the endoplasmic reticulum. *Nat. Commun.* **9**, 2939
22. Binns, D., Januszewski, T., Chen, Y., Hill, J., Markin, V. S., Zhao, Y. M., *et al.* (2006) An intimate collaboration between peroxisomes and lipid bodies. *J. Cell Biol.* **173**, 719–731
23. Thazar-Poulot, N., Miquel, M., Fobis-Loisy, I., and Gaude, T. (2015) Peroxisome extensions deliver the *Arabidopsis* SDP1 lipase to oil bodies. *Proc. Natl. Acad. Sci. U. S. A.* **112**, 4158–4163
24. Dirkx, R., Vanhorebeek, I., Martens, K., Schad, A., Grabenbauer, M., Fahimi, D., *et al.* (2005) Absence of peroxisomes in mouse

hepatocytes causes mitochondrial and ER abnormalities. *Hepatology* **41**, 868–878
25. Fan, C. Y., Pan, J., Chu, R., Lee, D., Kluckman, K. D., Usuda, N., *et al.* (1996) Hepatocellular and hepatic peroxisomal alterations in mice with a disrupted peroxisomal fatty acyl-coenzyme A oxidase gene. *J. Biol. Chem.* **271**, 24698–24710
26. Huyghe, S., Mannaerts, G. P., Baes, M., and Van Veldhoven, P. P. (2006) Peroxisomal multifunctional protein-2: the enzyme, the patients and the knockout mouse model. *Biochim. Biophys. Acta* **1761**, 973–994
27. Fan, W., Lam, S. M., Xin, J., Yang, X., Liu, Z., Liu, Y., *et al.* (2017) *Drosophila* TRF2 and TAF9 regulate lipid droplet size and phospholipid fatty acid composition. *PLoS Genet.* **13**, e1006664
28. Joo, H. J., Yim, Y. H., Jeong, P. Y., Jin, Y. X., Lee, J. E., Kim, H., *et al.* (2009) *Caenorhabditis elegans* utilizes dauer pheromone biosynthesis to dispose of toxic peroxisomal fatty acids for cellular homoeostasis. *Biochem. J.* **422**, 61–71
29. Xie, K., Zhang, P., Na, H., Liu, Y., Zhang, H., and Liu, P. (2019) MDT-28/PLIN-1 mediates lipid droplet-microtubule interaction via DLC-1 in *Caenorhabditis elegans*. *Sci. Rep.* **9**, 14902
30. Zhang, S. O., Box, A. C., Xu, N., Le Men, J., Yu, J., Guo, F., *et al.* (2010) Genetic and dietary regulation of lipid droplet expansion in *Caenorhabditis elegans*. *Proc. Natl. Acad. Sci. U. S. A.* **107**, 4640–4645
31. Watts, J. L., and Ristow, M. (2017) Lipid and carbohydrate metabolism in *Caenorhabditis elegans*. *Genetics* **207**, 413–446
32. Brooks, K. K., Liang, B., and Watts, J. L. (2009) The influence of bacterial diet on fat storage in *C. elegans*. *PLoS One* **4**, e7545
33. Zhang, P., Na, H., Liu, Z., Zhang, S., Xue, P., Chen, Y., *et al.* (2012) Proteomic study and marker protein identification of *Caenorhabditis elegans* lipid droplets. *Mol. Cell Proteomics* **11**, 317–328
34. Zhang, X., Feng, L., Chinta, S., Singh, P., Wang, Y., Nunnery, J. K., *et al.* (2015) Acyl-CoA oxidase complexes control the chemical message produced by *Caenorhabditis elegans*. *Proc. Natl. Acad. Sci. U. S. A.* **112**, 3955–3960
35. Zhang, X. X., Li, K. H., Jones, R. A., Bruner, S. D., and Butcher, R. A. (2016) Structural characterization of acyl-CoA oxidases reveals a direct link between pheromone biosynthesis and metabolic state in *Caenorhabditis elegans*. *Proc. Natl. Acad. Sci. U. S. A.* **113**, 10055–10060
36. Perez, C. L., and Van Gilst, M. R. (2008) A ^{13}C isotope labeling strategy reveals the influence of insulin signaling on lipogenesis in *C. elegans*. *Cell Metab.* **8**, 266–274
37. Watts, J. L., and Browse, J. (2002) Genetic dissection of polyunsaturated fatty acid synthesis in *Caenorhabditis elegans*. *Proc. Natl. Acad. Sci. U. S. A.* **99**, 5854–5859
38. Jeon, T. I., and Osborne, T. F. (2012) SREBPs: metabolic integrators in physiology and metabolism. *Trends Endocrinol. Metab.* **23**, 65–72
39. Kniazeva, M., Crawford, Q. T., Seiber, M., Wang, C. Y., and Han, M. (2004) Monomethyl branched-chain fatty acids play an essential role in *Caenorhabditis elegans* development. *PLoS Biol.* **2**, E257
40. Walker, A. K., Jacobs, R. L., Watts, J. L., Rottiers, V., Jiang, K., Finnegan, D. M., *et al.* (2011) A conserved SREBP-1/phosphatidylcholine feedback circuit regulates lipogenesis in metazoans. *Cell* **147**, 840–852
41. Yang, F., Vought, B. W., Satterlee, J. S., Walker, A. K., Jim Sun, Z. Y., Watts, J. L., *et al.* (2006) An ARC/Mediator subunit required for SREBP control of cholesterol and lipid homeostasis. *Nature* **442**, 700–704
42. Liang, B., Ferguson, K., Kadyk, L., and Watts, J. L. (2010) The role of nuclear receptor NHR-64 in fat storage regulation in *Caenorhabditis elegans*. *PLoS one* **5**, e9869
43. Martin, S., and Parton, R. G. (2006) Lipid droplets: a unified view of a dynamic organelle. *Nat. Rev. Mol. Cell Biol.* **7**, 373–378
44. Van Meer, G., Voelker, D. R., and Feigenson, G. W. (2008) Membrane lipids: where they are and how they behave. *Nat. Rev. Mol. Cell Bio.* **9**, 112–124
45. Shi, X., Li, J., Zou, X., Greggain, J., Rodkaer, S. V., Faergeman, N. J., *et al.* (2013) Regulation of lipid droplet size and phospholipid composition by stearoyl-CoA desaturase. *J. Lipid Res.* **54**, 2504–2514
46. Vrablik, T. L., Petyuk, V. A., Larson, E. M., Smith, R. D., and Watts, J. L. (2015) Lipidomic and proteomic analysis of *Caenorhabditis elegans* lipid droplets and identification of ACS-4 as a lipid droplet-associated protein. *Biochim. Biophys. Acta* **1851**, 1337–1345
47. Wilfling, F., Thiam, A. R., Olarte, M. J., Wang, J., Beck, R., Gould, T. J., *et al.* (2014) Arf1/COPI machinery acts directly on lipid droplets and enables their connection to the ER for protein targeting. *Elife* **3**, e01607
48. Koynova, R., and Caffrey, M. (1998) Phases and phase transitions of the phosphatidylcholines. *Biochim. Biophys. Acta* **1376**, 91–145
49. Herzog, K., Pras-Raves, M. L., Vervaart, M. A., Luyf, A. C., van Kampen, A. H., Wanders, R. J., *et al.* (2016) Lipidomic analysis of fibroblasts from Zellweger spectrum disorder patients identifies disease-specific phospholipid ratios. *J. Lipid Res.* **57**, 1447–1454
50. Herzog, K., Pras-Raves, M. L., Ferdinandusse, S., Vervaart, M. A. T., Luyf, A. C. M., van Kampen, A. H. C., *et al.* (2018) Functional characterisation of peroxisomal beta-oxidation disorders in fibroblasts using lipidomics. *J. Inherit. Metab. Dis.* **41**, 479–487
51. Zhang, J. J., Hao, J. J., Zhang, Y. R., Wang, Y. L., Li, M. Y., Miao, H. L., *et al.* (2017) Zinc mediates the SREBP-SCD axis to regulate lipid metabolism in *Caenorhabditis elegans*. *J. Lipid Res.* **58**, 1845–1854
52. Frokjaer-Jensen, C., Davis, M. W., Hopkins, C. E., Newman, B. J., Thummel, J. M., Olesen, S. P., *et al.* (2008) Single-copy insertion of transgenes in *Caenorhabditis elegans*. *Nat. Genet.* **40**, 1375–1383
53. Wu, J., Jiang, X., Li, Y., Zhu, T., Zhang, J., Zhang, Z., *et al.* (2018) PHA-4/FoxA senses nucleolar stress to regulate lipid accumulation in *Caenorhabditis elegans*. *Nat. Commun.* **9**, 1195
54. Lee, H. C., Inoue, T., Imae, R., Kono, N., Shirae, S., Matsuda, S., *et al.* (2008) *Caenorhabditis elegans mboa-7*, a member of the MBOAT family, is required for selective incorporation of polyunsaturated fatty acids into phosphatidylinositol. *Mol. Biol. Cell* **19**, 1174–1184
55. Lam, S. M., Zhou, T. X., Li, J., Zhang, S. H., Chua, G. H., Li, B. W., *et al.* (2020) A robust, integrated platform for comprehensive analyses of acyl-coenzyme as and acyl-carnitines revealed chain length-dependent disparity in fatty acyl metabolic fates across *Drosophila* development. *Sci. Bull.* **65**, 1840–1848
56. Mendel, M., Delaney, K., Pandey, R. R., Chen, K. M., Wenda, J. M., Vagbo, C. B., *et al.* (2021) Splice site m^{6}A methylation prevents binding of U2AF35 to inhibit RNA splicing. *Cell* **184**, 3125–3142